JBC RESEARCH ARTICLE

# AdipoRon exerts opposing effects on insulin sensitivity *via* fibroblast growth factor 21–mediated time-dependent mechanisms

Received for publication, November 17, 2021, and in revised form, January 19, 2022 Published, Papers in Press, January 25, 2022,
https://doi.org/10.1016/j.jbc.2022.101641

**Yongliang Wang[1], Huan Liu[1], Ruixin Zhang[1], Yuyao Xiang[1], Junfeng Lu[1], Bo Xia[1,*], Liang Peng[2,*], and Jiangwei Wu[1,*]**

*From the [1]Key Laboratory of Animal Genetics, Breeding and Reproduction of Shaanxi Province, College of Animal Science and Technology, Northwest A&F University, Yangling, Shaanxi, China; [2]Institute of Clinical Medical Sciences, China-Japan Friendship Hospital, Beijing, China*

Edited by Qi Qun Tang

**Increasing evidence has shown that AdipoRon, a synthetic adiponectin receptor agonist, is involved in the regulation of whole-body insulin sensitivity and energy homeostasis. However, the mechanisms underlying these alterations remain unclear. Here, using hyperinsulinemic–euglycemic clamp and isotopic tracing techniques, we show that short-term (10 days) AdipoRon administration indirectly inhibits lipolysis in white adipose tissue *via* increasing circulating levels of fibroblast growth factor 21 in mice fed a high-fat diet. This led to reduced plasma-free fatty acid concentrations and improved lipid-induced whole-body insulin resistance. In contrast, we found that long-term (20 days) AdipoRon administration directly exacerbated white adipose tissue lipolysis, increased hepatic gluconeogenesis, and impaired the tricarboxylic acid cycle in the skeletal muscle, resulting in aggravated whole-body insulin resistance. Together, these data provide new insights into the comprehensive understanding of multifaceted functional complexity of AdipoRon.**

Adiponectin, a cytokine produced by adipocytes (1), acts as a protective regulator because of its antilipotoxic, anti-inflammatory, and antiapoptotic properties (2). However, its expression levels are significantly decreased in obesity (3) and type 2 diabetes (4). Adiponectin administration is reported to ameliorate insulin resistance and glucose intolerance *via* activating the 5′ adenosine monophosphate–activated protein kinase (AMPK) (5, 6) and peroxisome proliferator–activated receptor α (PPARα) pathways (7) by binding to adiponectin receptor 1 and adiponectin receptor 2, respectively (8). Despite the beneficial effects of adiponectin on the regulation of metabolism and energy homeostasis, its complicated structure and rapid turnover limit its clinical application (2).

AdipoRon, an orally active synthetic small molecule, was identified as adiponectin receptor agonist that can bind to and activate both adiponectin receptor 1 and adiponectin receptor 2 (9). Similar to adiponectin, AdipoRon has many beneficial properties as a novel therapeutic agent for the treatment of metabolic-related diseases, such as type 2 diabetic nephropathy, *via* the activation of the $Ca^{2+}$/liver kinase B1–AMPK/PPARα pathway (10, 11). AdipoRon also plays a protective role in cardiac hypertrophy partly by activating AMPK-related pathways (12). Recent studies have demonstrated that oral administration or intraperitoneal injection of AdipoRon protects against postischemic myocardial apoptosis and secondary brain injury after intracerebral hemorrhage, which is possibly mediated by AMPK signaling (13, 14). In addition, a recent study has shown that oral administration of AdipoRon for 10 days increased fatty acid combustion and decreased oxidative stress and lipotoxicity in skeletal muscle and liver, which collectively improved insulin sensitivity and ameliorated glucose intolerance, thereby prolonging the shortened life span of diabetic mice (15). Hence, AdipoRon has been proposed as a potent energy regulator for the treatment of metabolic diseases. However, available data do not provide systemic mechanism underlying AdipoRon-mediated glucose homoeostasis, and whether the action of AdipoRon effectively and sustainably contributes to systemic energy homoeostasis is unclear.

In this study, we applied the hyperinsulinemic–euglycemic clamping method to assess whole-body insulin sensitivity of mice following short-term and long-term AdipoRon administration. The results showed that hepatic fibroblast growth factor 21 (FGF21) is linked to short-term AdipoRon-induced hepatic PPARα activation (10-day subcutaneous injection at 5 mg $kg^{-1}$ body weight [BW] per day), which improved glucose and lipid metabolism. Briefly, AdipoRon activates AdipoR–PPARα signaling, which increases hepatic FGF21 synthesis and secretion, leading to the suppression of lipolysis in white adipose tissue (WAT) and subsequent lower plasma levels of free fatty acids (FFAs), thus attenuating lipotoxicity of the liver and muscle and improving whole-body insulin sensitivity. However, long-term (20 days) AdipoRon treatment (5 mg $kg^{-1}$ BW per day) leads to a high rate of lipolysis in WAT, resulting in aggravated fatty liver and hepatic glucose production. Furthermore, persistent FGF21 activation by AdipoRon results in a sharp increase of circulating FGF21 compared with that in

* For correspondence: Bo Xia, imed23@nwafu.edu.cn; Liang Peng, pengliang8028@163.com; Jiangwei Wu, wujiangwei@nwafu.edu.cn.

short-term AdipoRon-treated mice, which impairs glucose disposal in the skeletal muscle and subsequently contributes to systemic insulin resistance.

## Results

### *Short-term administration of AdipoRon suppresses WAT lipolysis and improves glucose intolerance in mice fed a high-fat diet*

To investigate the effects of AdipoRon on high-fat diet (HFD)–induced insulin resistance, 8-week-old male mice were subcutaneously injected with AdipoRon (Fig. 1*A*). Despite neither BW, food intake, nor total fat and fat percentage were affected (Fig. 1, *B–E*), AdipoRon treatment improved HFD-induced whole-body glucose intolerance (Fig. 1, *F* and *G*) and reduced ectopic lipid accumulation in the liver associated with low protein levels of adipose triglyceride lipase (ATGL) and the ratio of phosphorylated hormone-sensitive lipase (p-HSL) to total HSL in WAT (Fig. 1, *H–J*). Consistently, AdipoRon reduced circulating FFA concentrations (Fig. 1*K*). These alterations suggest that AdipoRon improves lipid and glucose metabolism disorders in mice fed an HFD.

In contrast, 10-day AdipoRon treatment of mice fed the regular chow diet (RCD) (Fig. S1*A*) had no effect on the BW, total fat mass, fat percentage, fasting blood glucose levels (Fig. S1, *B–E*), glucose tolerance, or hepatic lipid content as compared with vehicle-treated control mice (Fig. S1, *F–H*). In addition, AdipoRon treatment had no effect on lipolysis-related protein levels of ATGL and the p-HSL:HSL ratio (Fig. S1, *I–J*). Furtherly, AdipoRon did not change the glucose infusion rate (GIR) during hyperinsulinemic–euglycemic mouse clamp (clamp) (Fig. S1, *K* and *L*). Tracer analysis showed that AdipoRon-treated mice displayed comparable whole-body glucose disposal in skeletal muscle and endogenous glucose production (EGP), in addition to EGP suppression, to dimethyl sulfoxide (DMSO) control mice (Fig. S1, *M–O*). Moreover, AdipoRon had no effects on FFA concentrations during fasting (basal) and clamping conditions, as well as FFA suppression (Fig. S1, *P* and *Q*), suggesting that

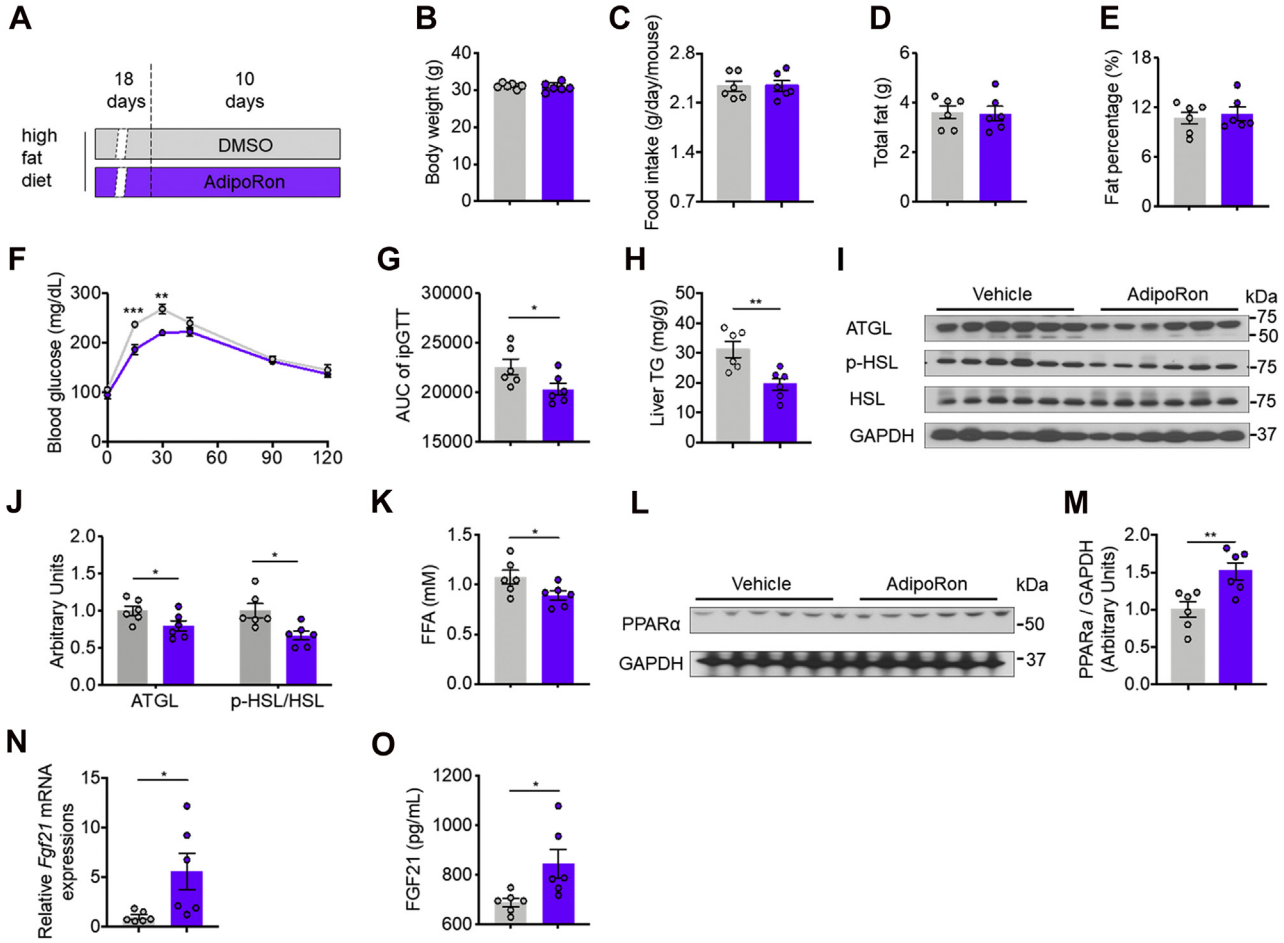


**Figure 1. AdipoRon treatment for 10 days improves HFD-induced glucose intolerance and lipid disorder.** *A*, diagram of the AdipoRon treatment regimen. Briefly, mice fed the HFD for 4 weeks were subcutaneously injected with AdipoRon (5 mg $kg^{-1}$ BW per day) or DMSO for the last 10 days of the HFD feeding period. *B*, BW. *C*, food intake. *D*, total fat. *E*, fat percentage. *F*, time course of blood glucose concentrations during the glucose tolerance test (GTT). *G*, area under the curve (AUC) of the GTT. *H*, hepatic TG contents. *I*, representative ATGL, p-HSL, and total HSL protein levels in WAT. *J*, quantification of ATGL and p-HSL/HSL protein expression. *K*, serum FFA concentrations. *L*, representative PPARα protein levels in the liver. *M*, quantification of PPARα protein expression. *N*, relative *Fgf21* mRNA expression in the liver. *O*, circulating FGF21 protein levels. ATGL, adipose triglyceride lipase; BW, body weight; DMSO, dimethyl sulfoxide; FFA, free fatty acid; *Fgf21*, fibroblast growth factor 21; HFD, high-fat diet; p-HSL, phosphorylated hormone-sensitive lipase; PPARα, peroxisome proliferator–activated receptor α; TG, triglyceride; WAT, white adipose tissue.

AdipoRon has no effect on glucose and lipid metabolism of mice fed the RCD.

Consistent with the results of previous studies, following AdipoRon treatment, PPARα protein levels were increased in the livers of mice fed an HFD diet (Fig. 1, *L* and *M*). Of note, AdipoRon increased hepatic *Fgf21* mRNA and circulating FGF21 levels (Fig. 1*O*).

### *Short-term administration of AdipoRon indirectly suppresses WAT lipolysis* via *activation of hepatic PPARα–FGF21 to improve whole-body insulin resistance*

Having observed elevated hepatic PPARα–*Fgf21* levels and circulating FGF21 levels, the effect of AdipoRon on direct regulation of the PPARα–FGF21 pathway in HFD-fed mice was investigated. A new cohort of HFD mice were raised and divided into three groups: vehicle, AdipoRon, and AdipoRon + FGF21-neutralizing antibody (Fig. 2*A*). The results showed that AdipoRon treatment elevated plasma FGF21 levels by 22.6% and decreased ectopic lipid accumulation in liver and skeletal muscle (gastrocnemius + solus) by 31.4% and 30.9%, respectively, whereas these increases were abolished by the neutralization of FGF21 with the anti-FGF21 antibody, as evidenced by the comparable plasma FGF21 concentrations and ectopic lipid contents of the vehicle and AdipoRon + anti-FGF21 groups (Fig. 2, *B–D*). Glucose tolerance test (GTTs) were performed to measure whole-body glucose tolerance, and interestingly, the results showed that AdipoRon-induced insulin sensitivity–improving effect was abolished by FGF21 neutralization, but not significantly (Fig. 2*E*). Next, to more specifically assess the potential impact of the PPARα–FGF21 pathway on the effect of AdipoRon, clamp was performed. AdipoRon-treated mice showed a marked increase in the GIR, suggesting improved HFD-induced whole-body insulin resistance. Nonetheless, neutralization of circulating FGF21 to a physiological level comparable to that of the vehicle group completely eliminated the insulin-sensitizing effect of AdipoRon (Fig. 2, *F* and *G*). Furthermore, AdipoRon lowered circulating FFA concentrations under fasting and clamping conditions without altering FFA suppression, which were associated with decreased levels of perilipin 1 (PLIN1) and monoacylglycerol lipase (MGL), two key proteins involved in WAT lipolysis. However, antibody neutralization of AdipoRon-induced FGF21 activation abrogated these effects (Fig. 2, *H–J*).

To further determine whether hepatic FGF21 links the action of AdipoRon to reduce adipose lipolysis, murine alpha mouse liver 12 (AML12) hepatocytes were treated with AdipoRon, and increased PPARα protein levels were observed (Fig. 2, *K* and *L*). Next, mature 3T3-L1 adipocytes were cocultured with AML12 cells pretreated with DMSO or AdipoRon in the presence or the absence of anti-FGF21 antibody (1.37 ng/ml) (Fig. 2*M*). Consistent with the *in vivo* results, AdipoRon significantly increased the FGF21 concentrations in the medium, whereas addition of the anti-FGF21 antibody sufficiently lowered the FGF21 content in the medium to a level similar to that of the vehicle group (Fig. 2*N*). Western blot analysis revealed lower protein levels of ATGL and MGL in the AdipoRon group than that in the vehicle control group, whereas FGF21 neutralization abrogated the suppression of lipolysis by AdipoRon, as evidenced by normalized protein levels of ATGL and MGL comparable to those of the vehicle group (Fig. 2, *O* and *P*). Furthermore, lipid accumulation was increased in pre-AdipoRon-treated AML12 cells cocultured with mature adipocytes and decreased in AML12 cells, whereas FGF21 neutralization abrogated these alterations, as shown by Oil Red O staining (Fig. 2, *Q* and *R*). These results suggest that AdipoRon indirectly suppresses WAT lipolysis *via* the activation of the hepatic PPARα–FGF21 axis to ameliorate diet-induced ectopic lipid accumulation and whole-body insulin resistance.

To validate *in vitro* findings, we treated HFD-fed FGF21 whole-body KO (FKO) mice with AdipoRon for 10 days (Fig. 3*A*). However, comparable BW and food intake were observed between control (FKO-vehicle) and AdipoRon (FKO-AdipoRon) groups (Fig. 3, *B* and *C*). In addition, clamp studies showed that AdipoRon did not change GIR, as well as EGP and whole-body glucose disposal (Fig. 3, *D–F*). Metabolic flux analysis in skeletal muscle showed that AdipoRon also did not change the ratio of $^{13}C_3$-pyruvate enrichments to plasma $^{13}C_3$-glucose enrichments, and the ratio of the enrichments of $^{13}C_3$-citrate, $^{13}C_2$-citrate, $^{13}C_2$-α-ketoglutarate, $^{13}C_2$-succinate, $^{13}C_2$-fumarate, $^{13}C_2$-malate, $^{13}C_3$-oxaloacetate, and $^{13}C_2$-oxaloacetate to $^{13}C_3$-pyruvate enrichments. Furtherly, AdipoRon-treated FKO mice displayed comparably the ratio of ($V_{\text{pyruvate dehydrogenase}}$) $V_{PDH}$ to ($V_{\text{pyruvate carboxylase}}$) $V_{PC}$, $V_{PC}$ and $V_{PDH}$ with vehicle mice in skeletal muscle (Fig. 3*G*).

Since FGF21 activation linked AdipoRon to lipolysis suppression in WAT, we next asked whether and how AdipoRon directly affects lipid metabolism. Incubation of 3T3-L1 cells with AdipoRon during adipogenesis markedly increased lipid accumulation in the AdipoRon group as compared with the DMSO control group (Fig. 4*A*). In addition, the mRNA expression levels of the adipogenesis-related genes *Glut4*, *Cidea*, *Cideb*, and *Cidec* were increased by AdipoRon to different degrees (Fig. 4, *C* and *D*). Although AdipoRon dramatically increased the mRNA levels of *Pnpla2* and *Lipe*, as well as *Cgi58*, PLIN1, and *perilipin 4*, but not *perilipin 3*, *perilipin 5*, *Ucp1*, and *Cpt1α* (Fig. 4, *E–G*), the protein levels of ATGL and pHSL remained unchanged. However, AdipoRon supplementation dramatically increased the protein levels of PPARγ and CEBPα, two key adipogenic transcription factors (Fig. 4, *H–J*). To further assess the direct impact of AdipoRon on lipolysis, differentiated muscle satellite cells were cocultured with differentiated adipocytes pretreated with DMSO, AdipoRon, or AdipoRon + FGF21 antibody (Fig. 4*K*). Although FGF21 concentrations were undetectable in the medium of all three groups (Fig. 4*L*), lipid accumulation was increased in both myoblasts (Fig. 4*M*) and AdipoRon-incubated and AdipoRon + anti-FGF21-incubated adipocytes as shown by Oil Red O staining (Fig. 4, *N* and *O*), reflecting AdipoRon *per se* can directly promote lipolysis.

To access the acute effect of AdipoRon on insulin action, using clamp, we acutely treated the HFD-fed mice with

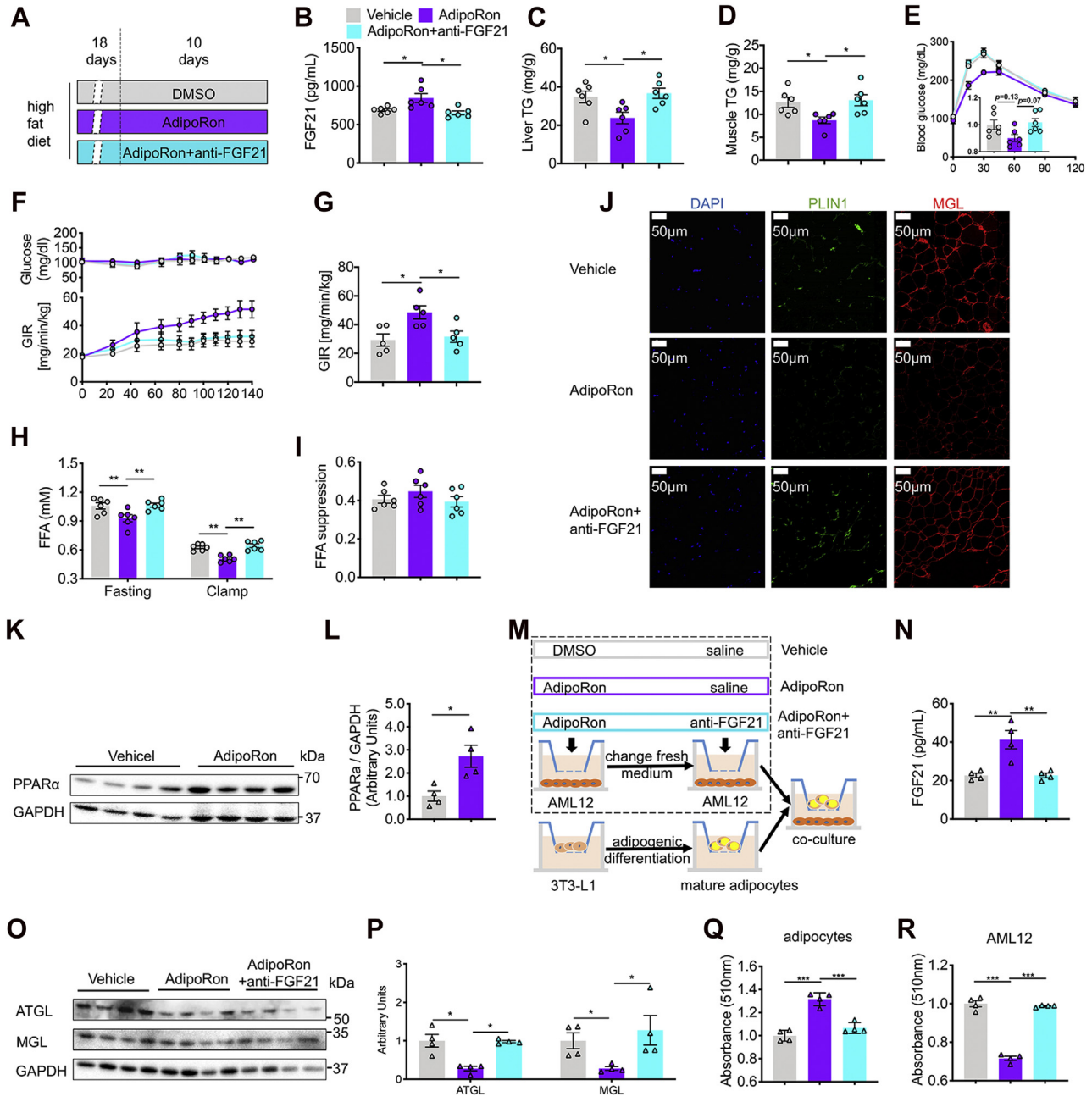


**Figure 2. FGF21 links to 10-day AdipoRon treatment and improved whole-body insulin sensitivity in mice fed the HFD.** *A*, diagram of the 10-day AdipoRon treatment regimen. Briefly, mice fed the HFD for 4 weeks were subcutaneously injected with DMSO or AdipoRon (5 mg $kg^{-1}$ BW per day) with or without the anti-FGF21 antibody (3.3 μg $kg^{-1}$ BW per day) for the last 10 days of the HFD feeding period. *B*, circulating FGF21 protein levels. *C* and *D*, hepatic and skeletal muscle (gastrocnemius and soleus) TG contents. *E*, time course of blood glucose concentrations during the glucose tolerance test. *F*, time course of blood glucose and the GIR during hyperinsulinemic–euglycemic clamping (clamp). *G*, the average GIR during a steady clamping state. *H*, circulating FFA concentrations in the fasting and clamping states. *I*, FFA suppression in mice fed the HFD. *J*, representative immunofluorescence (IF) images of PLIN1 and MGL in WAT. *K*, representative PPARα protein expression in AdipoRon-treated AML12 cells. *L*, quantification of PPARα. *M*, diagram of coculture regimen of AML12 and adipogenic-differentiated 3T3-L1 cells. Briefly, AML12 and 3T3-L1 cells were seeded in the *top* and *bottom wells*, respectively, of different transwell systems. The 3T3-L1 cells were differentiated into mature adipocytes. AML12 cells were treated with 23.3 μM AdipoRon or DMSO with or without 1.37 ng/ml of the anti-FGF21 antibody; then, the medium was replaced with DMEM containing 10% FBS until terminal differentiation of the 3T3-L1 cells was achieved. Then, the mature adipocytes seeded in the bottom well were cocultured with the AML12 cells seeded in the top well. *N*, FGF21 concentrations in the coculture medium. *O*, representative ATGL and MGL protein levels of AML12 cells. *P*, quantification of ATGL and MGL. *Q* and *R*, relative contents of Oil Red O in differentiated 3T3-L1 and AML12 cells. Briefly, after coculture studies, differentiated 3T3-L1 and AML12 cells were subjected to Oil Red O staining. Then, the Oil Red O was extracted with isopropyl alcohol, and the absorbances were measured with a multimode reader system. Data are presented as the mean ± SEM. *$p < 0.05$, **$p < 0.01$, and ***$p < 0.001$. AML12, alpha mouse liver 12; BW, body weight; DMSO, dimethyl sulfoxide; FBS, fetal bovine serum; FFA, free fatty acid; FGF21, fibroblast growth factor 21; GIR, glucose infusion rate; HFD, high-fat diet; MGL, monoacylglycerol lipase; PLIN1, perilipin 1; PPARα, peroxisome proliferator–activated receptor α; TG, triglyceride; WAT, white adipose tissue.

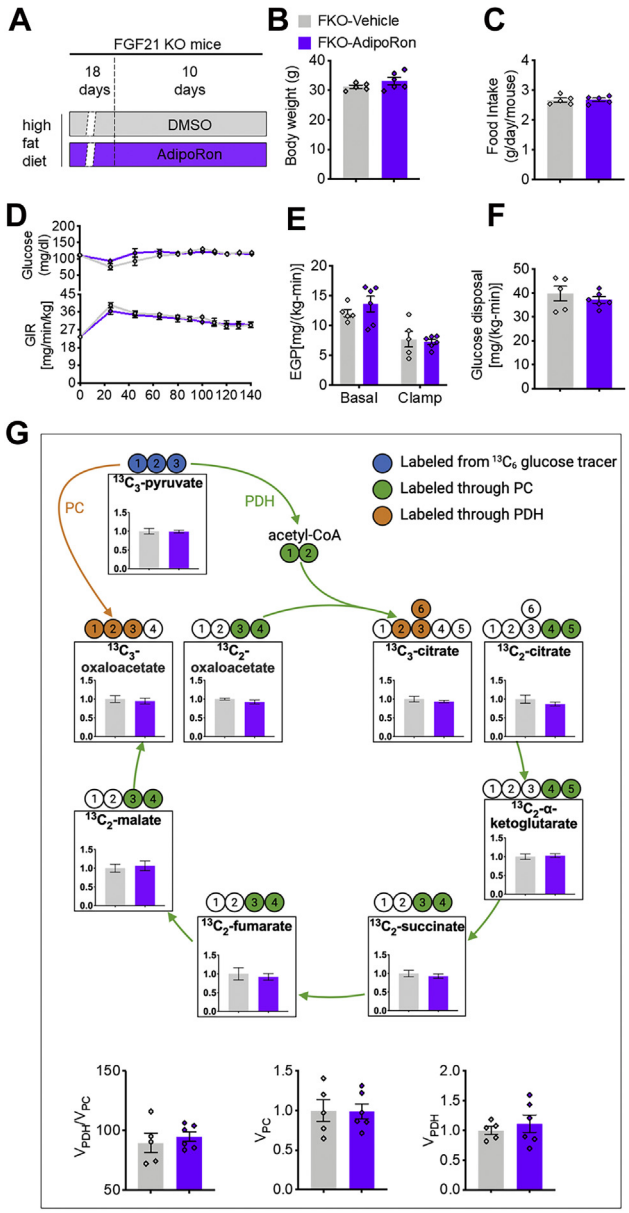


**Figure 3. AdipoRon has no effects on glucose metabolism in FGF21 KO mice.** *A*, diagram of the 10-day AdipoRon treatment regimen. Briefly, FGF21 KO mice fed the HFD for 4 weeks were subcutaneously injected with DMSO or AdipoRon (5 mg $kg^{-1}$ BW per day) for the last 10 days of the HFD feeding period. *B* and *C*, BW and food intake. *D*, time course of blood glucose and the GIR during clamp. *E*, endogenous glucose production (EGP) during basal infusion and clamp. *F*, whole-body glucose disposal. *G*, metabolic flux analysis in skeletal muscle (gastrocnemius and soleus). Data are presented as the mean ± SEM. BW, body weight; DMSO, dimethyl sulfoxide; FGF21, fibroblast growth factor 21; GIR, glucose infusion rate; HFD, high-fat diet.

AdipoRon. However, no difference in GIR was found between vehicle and AdipoRon groups (Fig. S2*A*). Furtherly, tracer assay demonstrated that AdipoRon did not change whole-body glucose disposal, basal and clamp EGP, as well as EGP suppression (Fig. S2, *B–D*).

Together, these data suggest that short-term, but not acute, AdipoRon administration improves whole-body insulin resistance *via* hepatic PPARα–FGF21-induced suppression of WAT lipolysis in mice fed the HFD.

### *Long-term administration of AdipoRon induced whole-body insulin resistance*

Next, the long-term impact of AdipoRon on systemic glucose homeostasis was investigated by treating mice fed the HFD with AdipoRon for 20 days (Fig. 5*A*). Consistent with previous findings, long-term AdipoRon administration increased circulating FGF21 concentrations by 14% (1599.59 ± 42.70 *versus* 1823.42 ± 24.53 pg/ml), whereas anti-FGF21 antibody decreased FGF21 to a level comparable to that of vehicle (DMSO)-treated mice (Fig. 5*B*). We found that AdipoRon, independent of circulating FGF21 concentrations, significantly increased the BW of mice in the AdipoRon (∼6.9%) and AdipoRon + anti-FGF21 groups (∼7.5%) (Fig. 5*C*). Consistently, increased food intake was observed in the AdipoRon (∼7.6%) and AdipoRon + anti-FGF21 groups (∼7.0%) (Fig. 5*D*) after 20 days of intervention. Although leptin is important for the regulation of food intake, leptin concentrations were similar among the three groups (Fig. 5*E*), thereby excluding the possible involvement of leptin in AdipoRon-induced appetite regulation. Although no changes were observed in alanine aminotransferase, aspartate aminotransferase, total cholesterol, triglycerides (TGs), high-density lipoprotein, and low-density lipoprotein concentrations among these groups, long-term AdipoRon treatment increased ectopic lipid accumulation in liver by 32.5% (Fig. 5, *F–I*), as well as in muscle by 21.4% (Fig. 5*J*), without changing fasting glucose and hepatic acetyl-CoA contents (Fig. 5, *K* and *L*). In contrast to improved insulin sensitivity by short-term AdipoRon administration, the insulin-sensitizing effect was abolished by long-term administration, as reflected by intraperitoneal GTT studies (Fig. 5, *M* and *N*). To gain further insight into insulin sensitivity, clamping was performed, which showed significantly decreased GIR in the long-term AdipoRon treatment group, whereas anti-FGF21 antibody partially rescued the insulin sensitivity–lowering action of AdipoRon, as reflected by reductions in the GIR of 27.3% and 15.5% in the AdipoRon and AdipoRon + anti-FGF21 groups, respectively (Fig. 5, *O* and *P*). Moreover, tracer analysis showed that clamp EGP was increased by 84.4% and 108.9%, whereas EGP suppression was reduced by 55.4% and 48.0% in the AdipoRon and AdipoRon + anti-FGF21 groups, respectively (Fig. 5, *Q* and *R*), with no difference in clamp EGP or EGP suppression between the AdipoRon and AdipoRon + anti-FGF21 groups. Interestingly, AdipoRon reduced glucose disposal by 13.6%, whereas the anti-FGF21 antibody completely rescued this phenomenon (Fig. 5*S*). Moreover, without altering fasting FFA concentrations, AdipoRon increased clamp FFA concentrations independent of FGF21, which was associated with increased expression levels of the lipolytic proteins PLIN1 and MGL in WAT (Fig. 5, *T* and *U*).

Since AdipoRon treatment progressively reduced glucose disposal, impairment of glycolysis or the tricarboxylic acid (TCA) cycle was expected in the skeletal muscle. To address this hypothesis, we performed metabolic flux analysis in skeletal muscle from clamped mice. AdipoRon increased the ratio of the enrichments of $^{13}C_2$-α-ketoglutarate to $^{13}C_3$-pyruvate

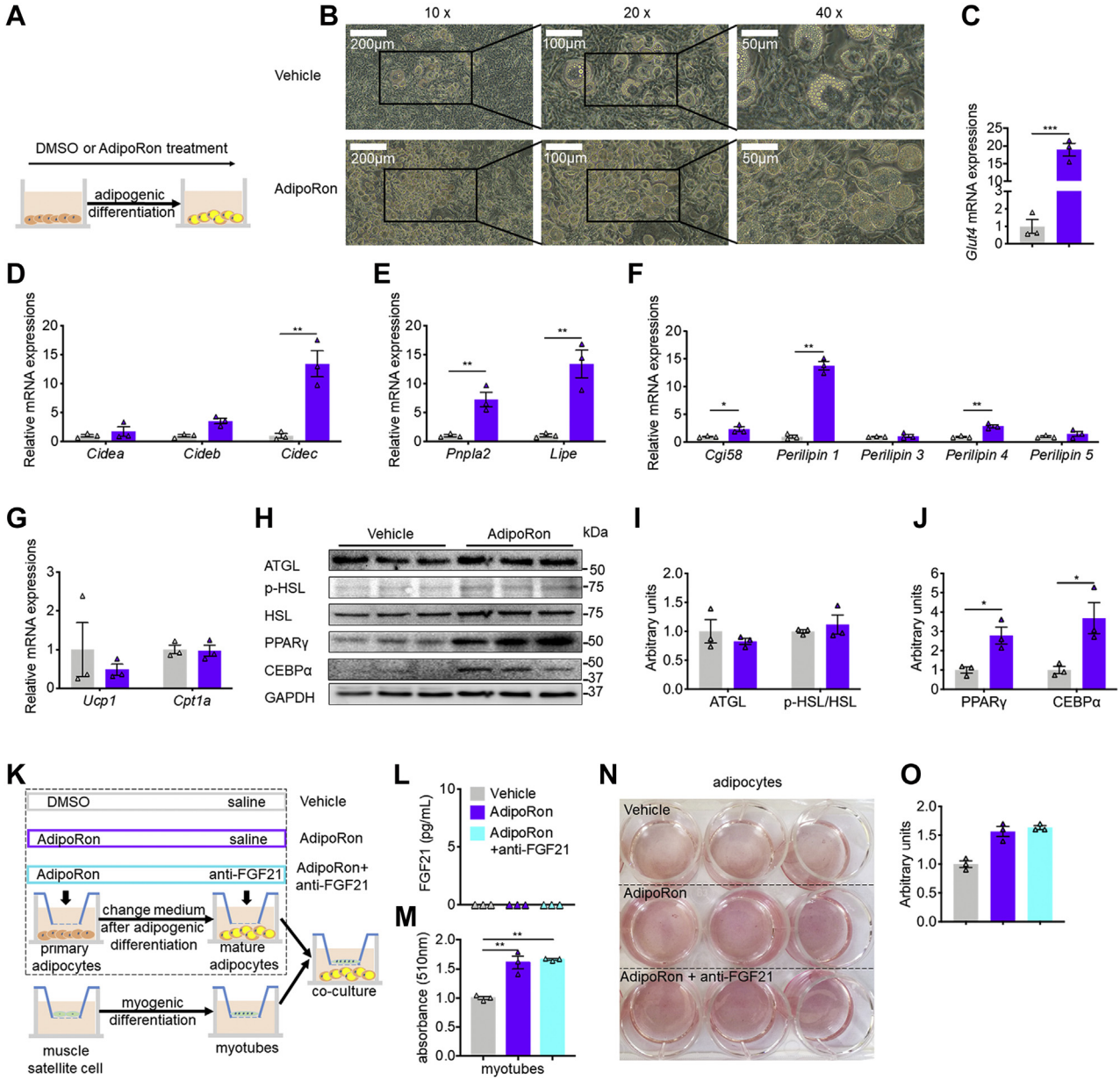


**Figure 4. AdipoRon treatment promotes adipogenesis and lipolysis *in vitro*.** *A*, diagram of the AdipoRon treatment regimen during 3T3-L1 adipogenic differentiation. *B*, representative images of adipogenic differentiation in 3T3-L1 cells. *C*, relative mRNA levels of Glut4. *D*, relative mRNA levels of Cide family. *E*, relative mRNA levels of Pnpla2 and Lipe. *F*, relative mRNA levels of lipolytic cofactors. *G*, relative mRNA levels of mitochondrial marker genes. *H*, representative protein levels of ATGL, p-HSL, total HSL, PPARγ, and CEBPα normalized to that of GAPDH. *I* and *J*, quantification of lipolysis-related and abiogenesis-related protein levels. *K*, diagram of coculture of primary adipocyte–derived mature adipocytes and muscle satellite cell–derived myofibers. Briefly, primary adipocytes and muscle satellite cells were seeded in the bottom and top wells of a transwell system, respectively, followed by adipogenic differentiation with DMSO, AdipoRon, or AdipoRon + anti-FGF21 antibody and myogenic differentiation. Then, the layers were resembled in a new coculture system. *L*, FGF21 concentrations in medium. *M*, relative contents of Oil Red O in myofibers. *N*, representative images of Oil Red O staining. *O*, relative contents of Oil Red O in differentiated 3T3-L1 cells. Data are presented as the mean ± SEM. $*p < 0.05$, $**p < 0.01$, and $***p < 0.001$. ATGL, adipose triglyceride lipase; CEBPα, CCAAT/enhancer-binding protein alpha; DMSO, dimethyl sulfoxide; p-HSL, phosphorylated hormone-sensitive lipase; PPARγ, peroxisome proliferator–activated receptor alpha.

enrichments, whereas decreased the enrichments of $^{13}C_2$-succinate to $^{13}C_3$-pyruvate enrichments without changing the ratio of $^{13}C_3$-pyruvate enrichment to plasma $^{13}C_3$-glucose enrichment, and the ratio of the enrichments of $^{13}C_3$-citrate, $^{13}C_2$-citrate, $^{13}C_2$-fumarate, $^{13}C_2$-malate, $^{13}C_3$-oxaloacetate, and $^{13}C_2$-oxaloacetate to $^{13}C_3$-pyruvate enrichment, as well as the ratio of $V_{PDH}$ to $V_{PC}$, $V_{PC}$ and $V_{PDH}$ (Fig. 5*V*). However, FGF21 antibody neutralization completely reversed these alterations. To further confirm these findings, DMSO-treated or AdipoRon-treated mice with or without the anti-FGF21 antibody were fasted overnight (from 6 PM to 10 AM) and then injected with 3 mmol/kg BW 2-deoxyglucose. We found that AdipoRon increased the contents of glucose metabolites, including glucose, glucose-1,6-bisphosphate, pyruvate, citrate, and α-ketoglutarate, in the skeletal muscle, but decreased the contents of succinate and fumarate, without changing malate

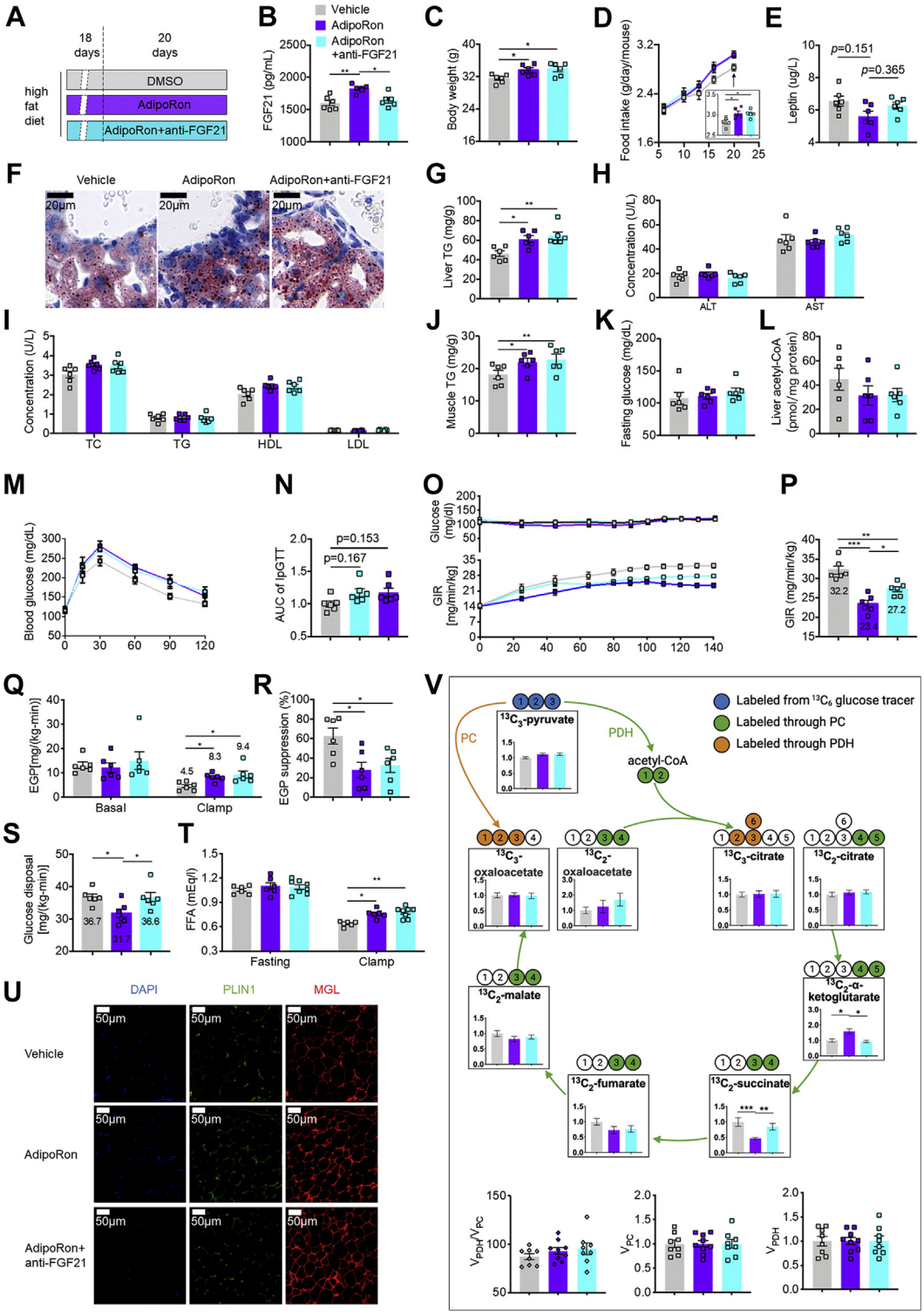


**Figure 5. AdipoRon treatment for 20 days exacerbated whole-body insulin resistance.** *A*, diagram of the AdipoRon treatment regimen *in vivo*. Briefly, mice fed the HFD for 18 days were subcutaneously injected with AdipoRon at 5 mg $kg^{-1}$ BW daily with or without the anti-FGF21 antibody (10.7 μg/mouse). DMSO-treated mice were used as vehicle controls. *B*, concentrations of circulating FGF21 in feeding mice. *C*, BW. *D*, time course of food intake after intervention. *E*, concentrations of circulating leptin in feeding mice. *F* and *G*, representative images of Oil Red O staining of the liver and hepatic lipid contents. *H* and *I*, serum concentrations of ALT, AST, TC, TG, HDL, and LDL. *J*, lipid contents in the skeletal muscle (gastrocnemius and soleus). *K*, fasting serum glucose concentrations. *L*, hepatic acetyl-CoA contents. *M*, time course of blood glucose concentrations during the GTT. *N*, AUC of the GTT. *O*, time course of blood glucose and the GIR during clamping. *P*, the GIR in the steady clamping state. *Q*, EGP during basal infusion and clamping. *R*, EGP suppression. *S*, whole-body glucose disposal rates. *T*, circulating FFA concentrations in the fasting and clamping states. *U*, representative IF images of PLIN1 and MGL in WAT. *V*, metabolic flux analysis in skeletal muscle (gastrocnemius and soleus). Data are presented as the mean ± SEM. *$p < 0.05$, **$p < 0.01$, and ***$p < 0.001$. ALT, alanine aminotransferase; AST, aspartate aminotransferase; AUC, area under the curve; BW, body weight; DMSO, dimethyl sulfoxide; EGP, endogenous glucose production; FFA, free fatty acid; FGF21, fibroblast growth factor 21; GIR, glucose infusion rate; GTT, glucose tolerance test; HDL, high-density lipoprotein; HFD, high-fat diet; IF, immunofluorescence; LDL, low-density lipoprotein; MGL, monoacylglycerol lipase; PLIN1, perilipin 1; TC, total cholesterol; TG, triglyceride; WAT, white adipose tissue.

contents (Fig. S3, *A–H*), suggesting an interruption of TCA flux by AdipoRon probably during the conversion of α-ketoglutarate to succinate. However, FGF21 antibody neutralization completely reversed the changes of these metabolites to levels comparable to those of the vehicle control group. Combined with similar concentrations of 2-deoxyglucose-6-phosphate, the metabolite of 2-deoxyglucose, among these groups (Fig. S3*I*), we deduced that AdipoRon impairs glucose utilization without affecting glucose uptake *via* the activation of hepatic FGF21 in the skeletal muscle in fasting condition.

To further understand the mechanism underlying the ability of AdipoRon to impair mitochondrial activity and subsequent glucose and lipid metabolism, the metabolic parameters of mice were assessed using the metabolic cage. The results showed that long-term AdipoRon treatment decreased whole-body-adjusted carbon dioxide production, but not oxygen consumption, in the dark and light hours or all day (Fig. 6, *A–F*). Consistently, the respiratory exchange rate was decreased in the dark hours, light hours, and all day (Fig. 6, *G–I*). Moreover, whole-body-adjusted energy expenditure (EE) was significantly reduced in the dark hours and all day, but not in the light hours (Fig. 6, *J–L*), whereas there was no change in physical activity (Fig. 6, *M–O*). Interestingly, AdipoRon increased whole-body-adjusted food intake in the dark hours, light hours, and all day (Fig. 6, *P–R*), with no difference in water consumption in the dark hours, light hours, and all day (Fig. 6, *S* and *T*). Consistent with the increase in food intake and reduction in EE, $^{1}$H magnetic resonance spectroscopy revealed dramatic increases in fat mass and fat percent (Fig. 6, *U* and *V*) but no change in lean mass (Fig. 6*W*).

## Discussion

Recent investigations have shown that the prevalence of diabetes in China, which has the largest number of patients with diabetes worldwide, dramatically increased from less than 1% in 1980 to more than 10% in 2013 (16), resulting in a tremendous public health burden. Although considerable progress has been made in understanding the molecular mechanisms underlying insulin resistance and type 2 diabetes, satisfactory treatment modalities remain limited. AdipoRon, an orally synthetic adiponectin receptor agonist, has also been investigated as a novel therapeutic agent for the treatment of type 2 diabetes (15). However, the underlying mechanism remains unclear, and whether the potential contribution of the sustained action of AdipoRon to systemic energy homoeostasis has not been investigated.

To understand the action of AdipoRon against metabolic disorders, diet-induced insulin-resistant mice were subcutaneously injected with AdipoRon daily for 10 days to examine the effect of short-term application on glucose and lipid metabolism. Consistent with the findings of a previous study (15), AdipoRon improved HFD-induced glucose intolerance, reduced ectopic lipid accumulation caused by suppression of WAT lipolysis, and subsequently reduced FFA flux in non-adipose tissues. In contrast, there was no difference in whole-body glucose tolerance, ectopic lipid accumulation, or lipolytic enzyme levels in mice fed the RCD following treatment with AdipoRon, suggesting that AdipoRon could improve glucose and lipid metabolism in individuals with energy disorders, but not healthy individuals.

Similar to previous data, PPARα protein levels were increased in the liver (15). PPARα has been identified as a critical regulator of hepatic lipid metabolism and energy homeostasis in response to fasting (17) and refeeding (18). Moreover, PPARα can directly induce FGF21 expression and increase circulating FGF21 levels (18, 19). As expected, AdipoRon administration induced FGF21 expression as reflected by increased circulating FGF21 concentrations in mice fed the HFD. Notably, FGF21 has also been ascribed as a key metabolic regulator, as exogenous FGF21 has glucose-lowering effects under glucose-loading conditions in diabetic models, and FGF21 transgenic mice were protected from Western diet–induced obesity in an insulin-dependent manner (20). Furthermore, FGF21 administration improved whole-body glucose and lipid metabolism *via* lipolysis suppression (21). Taken together, these data beg the question of whether AdipoRon improves glucose and lipid metabolism *via* hepatic FGF21. If so, neutralizing circulating FGF21 would be expected to block the actions of AdipoRon. Consistent with this hypothesis, *Fgf21* transcription levels and circulating FGF21 concentrations were higher in mice treated with AdipoRon. Furthermore, there was a dramatic improvement in glucose tolerance accompanied with reduced WAT lipolysis, as observed with the hyperinsulinemic–euglycemic clamping (clamp) method. However, in AdipoRon-treated mice, FGF21 neutralization completely eliminated the improvement in glucose metabolism, which was associated with rescued WAT lipolysis, suggesting that FGF21 is involved in the action of AdipoRon *via* the inhibition of WAT lipolysis. Consistently, short-term AdipoRon treatment–induced insulin-sensitizing effect found in wildtype mice was compromised in FGF21$^{+/-}$ mice, in addition to acute AdipoRon-treated mice. Notably, consistent with the findings *in vivo*, PPARα protein levels were also increased in AML12 hepatocytes pretreated with AdipoRon, suggesting that AdipoRon efficiently activated adiponectin receptor–PPARα signaling. To specifically confirm the effect of the PPARα–FGF21 axis on the actions of AdipoRon, AML12 hepatocytes pretreated with AdipoRon were cocultured with mature adipocytes. We observed reduced lipolysis in mature adipocytes and less lipid accumulation in AML12 cells associated with increased FGF21 protein contents in the medium, whereas these alterations were eliminated by FGF21 neutralization to match the FGF21 concentrations observed in control cells, validating that AdipoRon-induced activation of the PPARα–FGF21 axis is responsible for lipolysis suppression. Taken together, these data suggest that short-term, but not acute, AdipoRon treatment activates hepatic FGF21, thereby suppressing lipolysis in adipose tissue and decreasing circulating FFA levels, which contributed to improved fatty liver, decreased gluconeogenesis, and increased peripheral insulin sensitivity *in vivo*.

The indirect effects of AdipoRon were pivotal to lipid metabolism in WAT. Therefore, we posed the question of

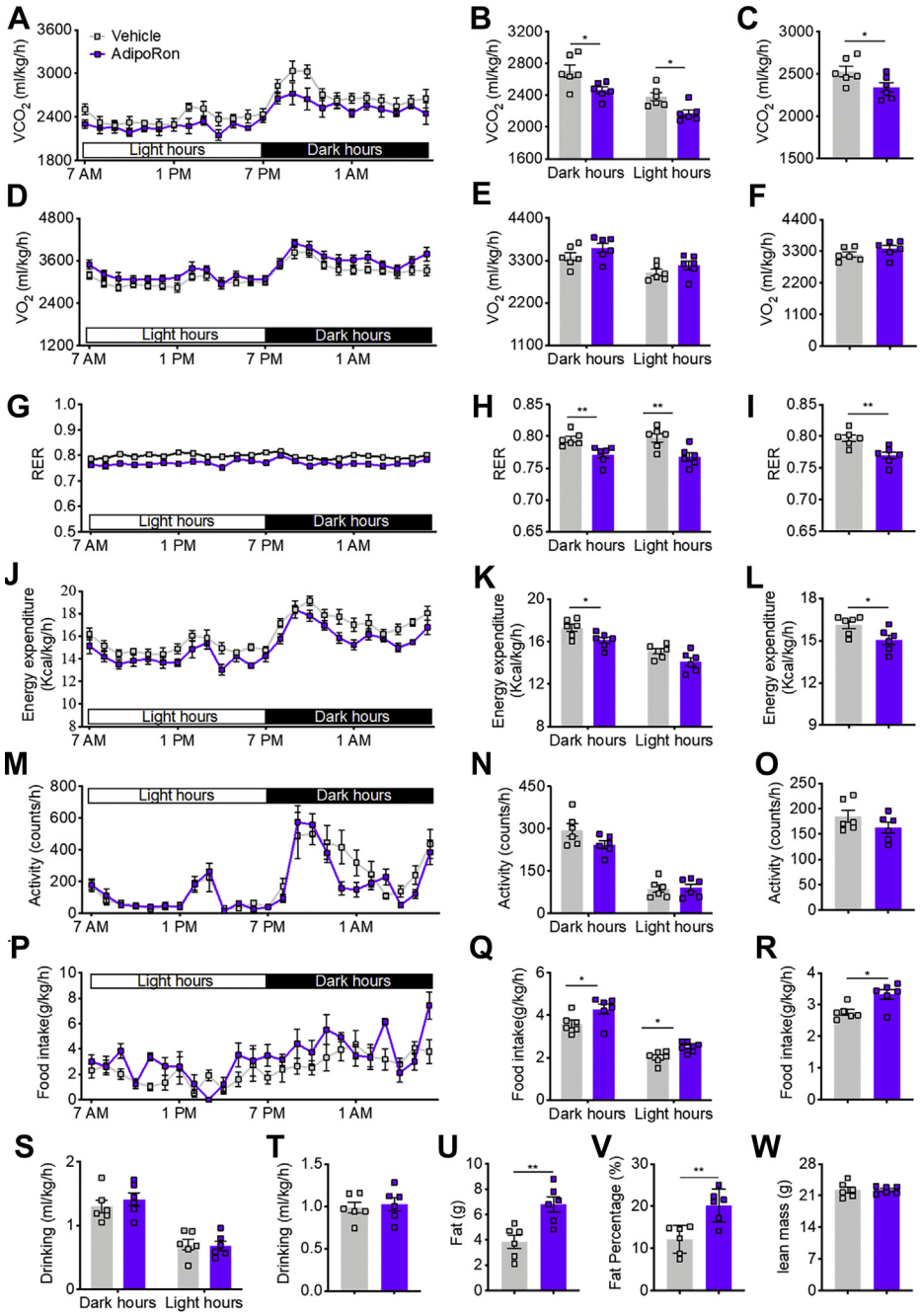


**Figure 6. AdipoRon treatment for 20 days reduced whole-body EE in mice fed the HFD.** *A*, time course of $VCO_2$. *B*, $CO_2$ production in dark and light hours. *C*, total $CO_2$ production. *D*, time course of $O_2$ consumption. *E*, $O_2$ consumption in dark and light hours. *F*, total $O_2$ consumption. *G*, time course of the RER. *H*, RER in dark and light hours. *I*, total RER. *J*, time course of EE. *K*, EE in dark and light hours. *L*, total EE. *M*, time course of physical activity. *N*, physical activity in dark and light hours. *O*, total activity. *M*, time course of EE. *N*, EE in dark and light hours. *O*, total EE. *P*, time course of food intake. *Q*, food intake in dark and light hours. *R*, total food intake. *S*, water intake in dark and light hours. *T*, total water intake. *U*, fat mass. *V*, fat percentage. *W*, lean mass. Data are presented as the mean ± SEM. $^*p < 0.05$ and $^{**}p < 0.01$. EE, energy expenditure; HFD, high-fat diet; RER, respiratory exchange rate; $VCO_2$, whole-body-adjusted carbon dioxide production.

whether AdipoRon directly regulates lipolysis *via* FGF21. To address this question, adipocytes were treated with AdipoRon during adipogenic differentiation. Unexpectedly, there were dramatic increases in the expression levels of adipogenesis-related genes, but not in lipolysis-related proteins, although the mRNA levels of lipolysis-related genes were increased. These data suggest that AdipoRon plays a role in post-transcriptional gene expression and might have no effect on FFA release. To test this hypothesis, mature adipocytes pre-treated with AdipoRon were cocultured with myotubes. Inconsistent with this possibility, there was a dramatic increase in lipid accumulation in the myotubes independent of FGF21, as reflected by undetectable FGF21 concentrations in the coculture medium in addition to no differences in lipid accumulation between the AdipoRon and AdipoRon + anti-FGF21 groups, suggesting that AdipoRon promotes the

activities of lipolysis-related enzymes with no change to protein levels. Taken together, these data demonstrate that AdipoRon can activate the hepatic PPARα–FGF21 axis, leading to lipolysis suppression in WAT, to achieve hepatic and peripheral insulin-sensitizing effects. Although AdipoRon can directly increase the activities of lipolysis-related enzymes independent of protein levels, increased FGF21 expression indirectly inhibits these activities *via* the liver–WAT axis.

Given the beneficial effects of AdipoRon on energy metabolism during short-term intervention and further considering the possibility that AdipoRon could be used to treat metabolic disorders, we next posed another question of whether AdipoRon could sustainably contribute to energy homeostasis. To answer these questions, mice fed the HFD were treated with AdipoRon for 20 days in the presence or the absence of the anti-FGF21 antibody to normalize circulating FGF21 levels (Fig. 5*A*). Previous data have suggested that leptin, as a key negative regulator of appetite, elicits a response from the brain to maintain sufficient fuel stores (22). In the present study, AdipoRon treatment increased food intake and BW in a leptin-independent and FGF21-independent manner without affecting lean mass. Consistently, AdipoRon also exacerbated whole-body insulin resistance, as reflected by decreased whole-body glucose disposal and increased hepatic glucose production. The former, but not the latter, was rescued by FGF21 normalization. Moreover, AdipoRon directly resulted in a remarkable increase in lipolysis in WAT independent of circulating FGF21 levels, as confirmed by *in vitro* studies. Together, the exacerbation of whole-body insulin resistance by long-term AdipoRon application can be likely explained by increased EGP driven by increased WAT lipolysis and subsequent increased PC activity, and decreased glucose disposal because of TCA cycle impairment by excessive FGF21 activation in the skeletal muscle. Despite exacerbating insulin resistance under insulin-loading conditions, AdipoRon had no effect on fasting glucose levels, which can be likely explained by the lack of changes in hepatic acetyl-CoA contents and PC activities and no subsequent change in hepatic glucose production.

Although FGF21 has been investigated as a potent therapeutic agent for insulin resistance, FGF21 concentrations increased with fasting (17), accompanied with worsening insulin resistance in the skeletal muscle in rodents (23), suggesting contrary functions of circulating FGF21 in response to different energy metabolism states. Consistently, short-term AdipoRon-induced FGF21 activation (from 689.4 pg/ml in vehicle mice to 845.4 pg/ml in AdipoRon-treated mice) was beneficial to whole-body glucose homeostasis, whereas excessive FGF21 activation by long-term AdipoRon treatment (from 1599.6 pg/ml in the vehicle group to 1823.4 pg/ml in the AdipoRon group) reduced glucose disposal because of impairment of the TCA cycle. Glucose metabolic flux analysis showed that long-term AdipoRon treatment impaired the conversion of α-ketoglutarate to succinate and thus impeded glycolysis and TCA flux. Consistently, long-term AdipoRon treatment lowered EE and promoted a shift from glucose to fat metabolism without changing activity. Taken together, these results reveal that long-term AdipoRon activates hepatic FGF21 and WAT lipolysis and mediates the glucose–fat cycle and interruption of the TCA cycle in the skeletal muscle, leading to insulin resistance in the skeletal muscle and liver. This may also explain the mechanism of peripheral insulin resistance under starvation conditions, in which fasting-induced hepatic FGF21 activation arrests the utilization of blood glucose *via* the suppression of the TCA cycle to ensure sufficient blood glucose supply to the brain under fasting conditions.

In summary, these data provide new insights into the beneficial effects of adiponectin receptor–activating agents on glucose metabolism and systemic insulin sensitivity (as shown in Fig. 7) as well as the adverse effects of long-term usage that may predispose patients to a risk of worsening metabolism disorders and clarify the clinical application of adiponectin receptor–targeted drugs.

## Experimental procedures

### *Cell models*

3T3-L1 and AML12 cells were purchased from the National Collection of Authenticated Cell Cultures. Upon arrival from the vendor, the cells were cultured in DMEM (Invitrogen) containing 10% FBS (Gibco) and passaged every 3 days. Primary adipocytes and muscle satellite cells were obtained from WAT and the gastrocnemius muscle of 8-week-old C57BL/6 male mice.

### *Animal models*

All animal studies were conducted in accordance with the approved guidelines of the Ethics Committee of Northwest A&F University. Eight-week-old C57BL/6J male mice were purchased from the Animal Center of Xi'An Jiao Tong University, and FGF21 heterogeneous mice were purchased from Cyagen Biosciences. Upon arrival, the mice were housed under a 12-h light/dark cycle at a controlled temperature of 23 to 24 °C with free access to water and an RCD (catalog no.: 1025; Beijing HFK Bioscience Co, Ltd) or 60% calorie HFD (catalog no.: H10060; Beijing HFK Bioscience Co, Ltd).

### *AdipoRon treatment*

For short-term AdipoRon treatment, 8-week-old male mice were provided the RCD or HFD for 4 weeks and subcutaneously injected with DMSO or AdipoRon (5 mg $kg^{-1}$ BW per day) with or without the anti-FGF21 antibody (3.3 μg $kg^{-1}$ BW per day) during the last 10 days of the HFD period.

For long-term AdipoRon treatment, 8-week-old male mice were provided the RCD or HFD for 18 days and subcutaneously injected with AdipoRon (5 mg $kg^{-1}$ BW per day) with or without the anti-FGF21 antibody (10.7 μg $kg^{-1}$ BW per day) for 20 days.

### *Body composition*

Mouse BW was measured with an electronic analytical balance (HT-80E; Cibio-tech), and body fat content was

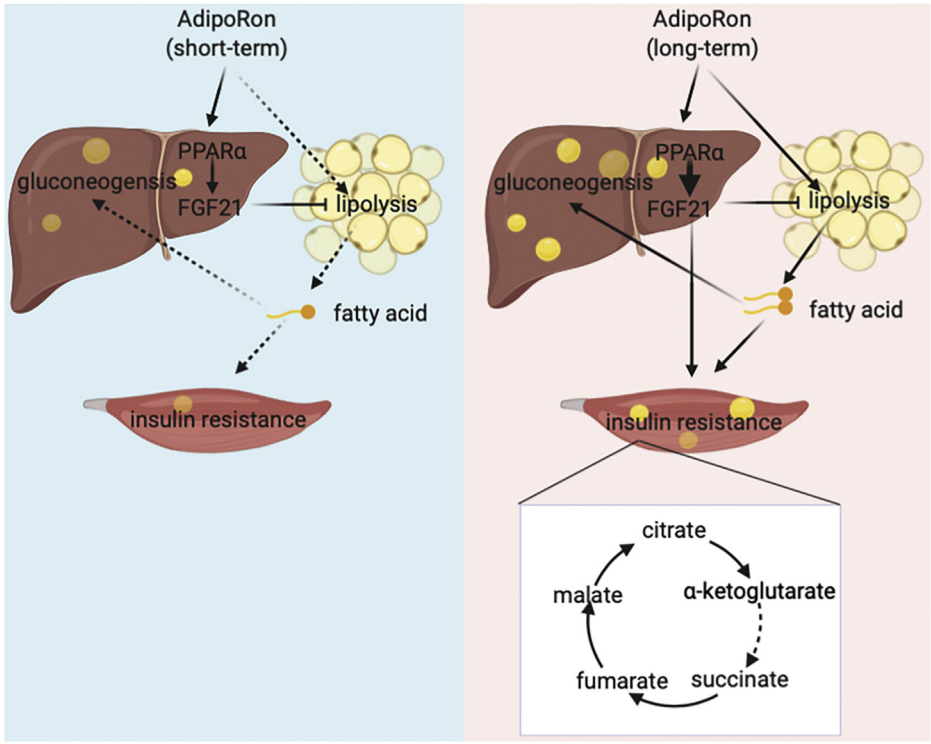


**Figure 7. Suggested mechanism by which AdipoRon application regulates glucose and lipid metabolism.** Briefly, short-term AdipoRon indirectly suppresses lipolysis in adipose tissue *via* activating circulating FGF21 in HFD-fed mice, leading to nonesterified fatty acid reduction and whole-body insulin resistance improvement. In contrast, long-term AdipoRon treatment directly exacerbates adipose tissue lipolysis, thus resulting in increased hepatic gluconeogenesis and impaired TCA cycle in skeletal muscle, causing aggravated systemic insulin resistance. FGF21, fibroblast growth factor 21; HFD, high-fat diet; TCA, tricarboxylic acid.

assessed by $H^1$ magnetic resonance spectroscopy (Bruker BioSpin).

### *GTT*

Following overnight (from 6 PM to 9 AM) fasting, the mice fed the RCD or HFD for 4 weeks were placed in a rat-size restrainer with the tail tape-tethered for 1 h for acclimatization to a partially restrained state. Then, the mice were intraperitoneally injected with 1.1 g/kg BW (RCD group) or 1 g/kg BW (HFD group) of 20% dextrose, and blood glucose concentrations were measured at 0, 15, 30, 45, 60, 90, and 120 min afterward.

### *Biochemical analysis*

Plasma nonesterified FAs were measured using commercial reagents (Wako Diagnostics). Plasma alanine aminotransferase, aspartate aminotransferase, total cholesterol, TG, high-density lipoprotein, and low-density lipoprotein levels were measured in Yangling Demonstration Zone Hospital. Plasma FGF21 and leptin levels were measured using commercial ELISA kits (R&D Systems). Tissue TG contents were extracted as previously described (24) and measured with TG-SL reagent (Sekisui).

### *Metabolic cage study*

Whole-body adjusted carbon dioxide production, oxygen consumption, respiratory exchange rate, EE, activity, food intake, and water intake were measured using a computer system as previously described (24).

### *Metabolite measurement and metabolic flux assay*

For the AdipoRon treatment studies, overnight-fasted 20-day DMSO, AdipoRon, and AdipoRon + anti-FGF21 antibody-pretreated mice were subcutaneously injected with 3 mmol/kg BW of 2-deoxyglucose and sacrificed at 15 min after injection. Skeletal muscles (gastrocnemius and soleus) were collected for measurement of TCA substrates and 2-deoxyglucose-6-phosphate by LC–MS.

For metabolic flux analysis, LC–MS was used to determine the enrichments of plasma glucose (*m/z* 180 [m + 0], 186 [m + 6]), pyruvate (*m/z* 87 [m + 0], 90 [m + 3]), citrate (*m/z* 191 [m + 0], 192 [m + 2], 194[m + 3]), α-ketoglutarate (*m/z* 145 [m + 0], 147 [m + 2]), succinate (*m/z* 117 [m + 0], 119 [m + 2]), fumarate (*m/z* 115 [m + 0], 117 [m + 2]), malate (*m/z* 133 [m + 0], 135 [m + 2]), and oxaloacetate (*m/z* 130 [m + 0], 132 [m + 2]), and 133 [m + 3]). The relative enrichment of pyruvate was measured as the ratio of $[^{13}C_3]$ pyruvate/$[^{13}C_6]$ glucose. The TCA cycle metabolite enrichments were normalized by the $[^{13}C_3]$ pyruvate enrichment. Following clamp, $[^{13}C_3]$ pyruvate arises from glycolysis of $[^{13}C_6]$ glucose and then enters the TCA cycle through PDH or through PC. [m + 2] malate was regarded as a readout for PDH activity, and [m + 3] malate was regarded as a readout for PC activity. The relative $V_{PC}$ was measured as the ratio of [m + 3] malate/$[^{13}C_3]$ pyruvate. The

$V_{PDH}/V_{PC}$ flux was measured as the ratio of [m + 2] malate/[m + 3] malate.

For the FGF21 KO mice studies, FGF21 KO and wildtype mice were placed in a rat-size restrainer with the tail tape-tethered for 1 h. Following overnight fasting, blood samples were collected from the tail vein for fasting glucose measurements. Afterward, the mice were sacrificed, and skeletal muscles were collected for measurement of α-ketoglutarate, succinate, and palmitate contents.

### *Hyperinsulinemic–euglycemic mouse clamp (clamp)*

Clamp studies were performed by Yangling IDimple Biotechnology Co, Ltd (request for technical support *via* enquiries: e-mail idimple@163.com). Briefly, the mice were implanted with sterile catheter in the jugular vein and then individually housed for recovering for 7 days before clamping. After then, the mice were fasted overnight (from 6 PM to 8 AM) and then infused with [U–$^{13}C_6$]-glucose (ZCI-CLM-1396; Shanghai Zzbio Co, Ltd) at a rate of 3.93 μg/min (and AdipoRon at a rate of 76.89 pmol/min only for acute AdipoRon treatment clamp studies) for 120 min. After basal glucose (16-h fasted blood glucose) sampling, clamps were conducted for 140 min with a 3-min primed infusion of insulin (6.0 mU/[kg-min]), followed by a continuous insulin infusion (2.5 mU/[kg-min) and 5 μg/min (U–$^{13}C_6$)-glucose (and AdipoRon at a rate of 76.89 pmol/min only for acute AdipoRon treatment clamp studies) as well as a variable infusion of 20% dextrose to maintain euglycemia (∼120 mg/dl). After that, the mice were sacrificed with a sodium pentobarbital intravenous injection, and then the blood and tissue samples were taken. The tissue samples were preserved in 4% paraformaldehyde for immunofluorescence analysis or snap-frozen in liquid nitrogen for future analysis.

### *Tracer analysis*

Whole-body glucose turnover rates (basal EGP and glucose disposal) were calculated as follows:

$$Glucose\ turnover = \left(\frac{Infusate\ C^{13}\ enrichment}{Plasma\ C^{13}\ enrichment} - 1\right) * infusion\ rate$$

$C^{13}$ enrichment ([U–$^{13}C_6$]-glucose enrichment) was measured as previously described (23). Briefly, 10 μl of each plasma sample was deprotonized with 25 μl of 10 mM $Ba(OH)_2$ and 25 μl of 10 mM $ZnSO_4$ and then derivatized with 50 μl of acetic anhydride and an equal volume of pyridine at 65 °C for 15 min. Afterward, the reaction was quenched with 100 μl of methanol. Then, $C^{13}$ enrichment was measured using gas chromatography–mass spectrometry in chemical ionization mode.

The clamp EGP was calculated as follows:

$$Clamp\ EGP = glucose\ disposal - glucose\ infusion\ rate$$

### In vitro *studies*

For coculture of AML12 and differentiated 3T3-L1 cells, AML12 and 3T3-L1 cells were plated in the top and bottom wells, respectively, of a transwell coculture system (Fig. 2*M*). The 3T3-L1 cells were differentiated with standard adipogenic medium. Meanwhile, AML12 cells were incubated in DMEM containing 10% FBS with 23.3 μM AdipoRon or DMSO. After 6 days, the differentiated 3T3-L1 cells seeded in the bottom well and the AML12 cells seeded in the top well were cocultured in medium containing 10% FBS with or without 1.37 ng/ml of anti-FGF21 antibody for 12 h.

For AdipoRon treatment, 3T3-L1 cells were plated in the wells of 6-well plates and then incubated with standard adipogenic medium as previously described (25) or the same medium containing 23.3 μM AdipoRon for 6 days.

For coculture of mature adipocytes and myotubes, muscle satellite cells and primary adipocytes obtained from wildtype C57BL/6J male mice were plated in the top and bottom wells, respectively, of a transwell coculture system (Fig. 2*M*). The muscle satellite cells were differentiated with standard myogenic medium as previously described (26), whereas the primary adipocytes were differentiated with standard adipogenic medium with or without 23.3 μM AdipoRon. After 6 days, the differentiated muscle satellite cells seeded in the bottom well and the mature adipocytes seeded in the top well were cocultured in medium containing 10% FBS with or without 1.37 ng/ml of anti-FGF21 antibody for 12 h.

### *RNA extraction and quantitative PCR*

Total RNA was extracted using a DNA/RNA/protein kit (catalog no.: R6734; OMEGA) in accordance with the manufacturer's protocol and then reverse transcribed into complementary DNA with a Prime Script first Strand cDNA Synthesis Kit (catalog no.: 6110A; TAKARA) and amplified by quantitative PCR with a CFX96 Real-Time System (Bio-Rad Laboratories).

### *Immunofluorescence and Western blot analyses*

Immunofluorescence analysis was performed as previously described (27), with a light microscope (Leica DM6B; Leica) in the Life Science Research Core Services in Northwest Agriculture and Forestry University. For Western blot analysis, tissues were homogenized in prechilled radioimmunoprecipitation assay buffer (Beyotime Biotechnology) and centrifuged to collected supernatant at 13,000*g* at 4 °C for 15 min. Then, 20 μg of total protein was loaded into the wells of SDS gels and resolved by PAGE; it was then transferred to polyvinylidene fluoride membranes (Millipore) using a semidry transfer system (Bio-Rad). After blocking for

1 h with 5% skim milk, the membranes were incubated overnight with primary antibodies. After washing twice, the membranes were incubated with horseradish peroxidase–conjugated secondary antibody for 2 h. Immune complexes were detected using a luminol chemiluminescence system (Thermo Fisher Scientific). Detecting reagents, including anti-FGF21 (catalog no.: sc81946; 1:1000 dilution), anti-PPARα (catalog no.: sc398394; 1:1000 dilution), ant-PLIN1 (catalog no.: sc390169; 1:1000 dilution), anti-MGL (catalog no.: sc398942; 1:1000 dilution), and anti-PPARγ (catalog no.: sc166731; 1:1000 dilution), were purchased from Santa Cruz Biotechnology. Anti-ATGL (catalog no.: 24395; 1:3000 dilution), anti-p-HSL (catalog no.: 4107T; 1:3000 dilution), anti-HSL (catalog no.: 4139; 1:3000 dilution), and anti-GAPDH (catalog no.: 5174T; 1:3000 dilution) were purchased from Cell Signaling Technology and anti-CEBPα (catalog no.: ab40764; 1:3000 dilution) was purchased from Abcam.

### *Oil Red O staining*

Fresh liver samples were fixed in 4% paraformaldehyde. Frozen sections were stained with Oil Red O as previously described (25). Nuclei were stained with hematoxylin.

### *Quantification and statistical analysis*

Data are presented as the mean ± SEM. The unpaired Student's $t$ test was used to calculate probability ($p$) values. A $p < 0.05$ was considered statistically significant. Multifactorial analysis of variance was used for statistical comparisons of more than two groups. GraphPad Prism 9 (GraphPad Software, Inc) was used for all statistical analyses.

## Data availability

Further information and requests for resources and reagents should be directed to and will be fulfilled by the lead contact, Jiangwei Wu (wujiangwei@nwafu.edu.cn).

*Supporting information*—This article contains supporting information.

*Acknowledgments*—We thank all members of our laboratory for their help. This work was supported by the National Key Research and Development Program of China (grant no.: 2021YFF1000602), National Natural Science Foundation of China (grant nos.: 31902137, 81970713, and 82170817), Beijing Municipal Natural Science Foundation of China (grant no.: 7222160), and Chinese Universities Scientific Fund (grant no.: 2452018049) from Northwest A&F University. We also thank the Life Science Research Core Services NWAFU (Xiaorui Liu) for assistance with immunofluorescence.

*Author contributions*—Y. W., B. X., L. P., and J. W. conceptualization; Y. W., H. L., R. X., Y. X., J. L., and X. Q. validation; Y. W., H. L., R. X., Y. X., J. L., and X. Q. formal analysis; Y. W. investigation; B. X., L. P., and J. W. resources; Y. W., H. L., R. X., Y. X., J. L., and X. Q. data curation; Y. W. writing–original draft; B. X., L. P., and J. W. writing–review & editing; Y. W., H. L., R. X., Y. X., J. L., and X. Q. visualization; B. X., L. P., and J. W. supervision; B. X., L. P., and J. W. project administration; Y. W., L. P., and J. W. funding acquisition.

*Conflict of interest*—The authors declare that they have no conflicts of interest with the contents of this article.

*Abbreviations*—The abbreviations used are: AML12, alpha mouse liver 12; AMPK, adenosine monophosphate–activated protein kinase; ATGL, adipose triglyceride lipase; BW, body weight; DMSO, dimethyl sulfoxide; EE, energy expenditure; EGP, endogenous glucose production; FFA, free fatty acid; FGF21, fibroblast growth factor 21; FKO, FGF21 whole-body knockoutGIR, glucose infusion rate; GTT, glucose tolerance test; HFD, high-fat diet; MGL, monoacylglycerol lipase; p-HSL, phosphorylated hormone-sensitive lipase; PLIN1, perilipin 1; PPARα, peroxisome proliferator–activated receptor α; RCD, regular chow diet; TCA, tricarboxylic acid; TG, triglyceride; $V_{PC}$, $V_{pyruvate\ carboxylase}$; $V_{PDH}$, $V_{pyruvate\ dehydrogenase}$; WAT, white adipose tissue.

## References

1. Scherer, P. E., Williams, S., Fogliano, M., Baldini, G., and Lodish, H. F. (1995) A novel serum protein similar to C1q, produced exclusively in adipocytes. *J. Biol. Chem.* **270**, 26746–26749
2. Holland, W. L., and Scherer, P. E. (2013) Cell Biology. Ronning after the adiponectin receptors. *Science* **342**, 1460–1461
3. Arita, Y., Kihara, S., Ouchi, N., Takahashi, M., Maeda, K., Miyagawa, J.-i., Hotta, K., Shimomura, I., Nakamura, T., Miyaoka, K., Kuriyama, H., Nishida, M., Yamashita, S., Okubo, K., Matsubara, K., *et al.* (1999) Paradoxical decrease of an adipose-specific protein, adiponectin, in obesity. *Biochem. Biophys. Res. Commun.* **257**, 79–83
4. Hotta, K., Funahashi, T., Arita, Y., Takahashi, M., Matsuda, M., Okamoto, Y., Iwahashi, H., Kuriyama, H., Ouchi, N., Maeda, K., Nishida, M., Kihara, S., Sakai, N., Nakajima, T., Hasegawa, K., *et al.* (2000) Plasma concentrations of a novel, adipose-specific protein, adiponectin, in type 2 diabetic patients. *Arterioscler. Thromb. Vasc. Biol.* **20**, 1595–1599
5. Yamauchi, T., Kamon, J., Minokoshi, Y., Ito, Y., Waki, H., Uchida, S., Yamashita, S., Noda, M., Kita, S., Ueki, K., Eto, K., Akanuma, Y., Froguel, P., Foufelle, F., Ferre, P., *et al.* (2002) Adiponectin stimulates glucose utilization and fatty-acid oxidation by activating AMP-activated protein kinase. *Nat. Med.* **8**, 1288–1295
6. Tomas, E., Tsao, T.-S., Saha, A. K., Murrey, H. E., Zhang, C.c., Itani, S. I., Lodish, H. F., and Ruderman, N. B. (2002) Enhanced muscle fat oxidation and glucose transport by ACRP30 globular domain: Acetyl–CoA carboxylase inhibition and AMP-activated protein kinase activation. *Proc. Natl. Acad. Sci. U. S. A.* **99**, 16309–16313
7. Kersten, S., Desvergne, B., and Wahli, W. (2000) Roles of PPARs in health and disease. *Nature* **405**, 421–424
8. Yamauchi, T., Nio, Y., Maki, T., Kobayashi, M., Takazawa, T., Iwabu, M., Okada-Iwabu, M., Kawamoto, S., Kubota, N., Kubota, T., Ito, Y., Kamon, J., Tsuchida, A., Kumagai, K., Kozono, H., *et al.* (2007) Targeted disruption of AdipoR1 and AdipoR2 causes abrogation of adiponectin binding and metabolic actions. *Nat. Med.* **13**, 332–339
9. Okada-Iwabu, M., Iwabu, M., Ueki, K., Yamauchi, T., and Kadowaki, T. (2015) Perspective of small-molecule AdipoR agonist for type 2 diabetes and short life in obesity. *Diabetes Metab. J.* **39**, 363–372
10. SR, C., JH, L., MY, K., EN, K., Y, K., BS, C., YS, K., HW, K., KM, L., MJ, K., and CW, P. (2018) Adiponectin receptor agonist AdipoRon decreased ceramide, and lipotoxicity, and ameliorated diabetic nephropathy. *Metabolism* **85**, 348–360
11. Iwabu, M., Okada-Iwabu, M., Yamauchi, T., and Kadowaki, T. (2019) Adiponectin/AdipoR research and its implications for lifestyle-related diseases. *Front. Cardiovasc. Med.* **6**, 116
12. Hu, X., Ou-Yang, Q., Wang, L., Li, T., Xie, X., and Liu, J. (2018) AdipoRon prevents l-thyroxine or isoproterenol-induced cardiac hypertrophy

through regulating the AMPK-related pathway. *Acta Biochim. Biophys. Sin. (Shanghai)* **51**, 20–30
13. Zhang, Y., Zhao, J., Li, R., Lau, W. B., Yuan, Y. X., Liang, B., Li, R., Gao, E. H., Koch, W. J., Ma, X. L., and Wang, Y. J. (2015) AdipoRon, the first orally active adiponectin receptor activator, attenuates postischemic myocardial apoptosis through both AMPK-mediated and AMPK-independent signalings. *Am. J. Physiol. Endocrinol. Metab.* **309**, E275–E282
14. Yu, J., Zheng, J., Lu, J., Sun, Z., Wang, Z., and Zhang, J. (2019) AdipoRon protects against secondary brain injury after intracerebral hemorrhage via alleviating mitochondrial dysfunction: Possible involvement of AdipoR1-AMPK-PGC1α pathway. *Neurochem. Res.* **44**, 1678–1689
15. Okada-Iwabu, M., Yamauchi, T., Iwabu, M., Honma, T., Hamagami, K., Matsuda, K., Yamaguchi, M., Tanabe, H., Kimura-Someya, T., Shirouzu, M., Ogata, H., Tokuyama, K., Ueki, K., Nagano, T., Tanaka, A., *et al.* (2013) A small-molecule AdipoR agonist for type 2 diabetes and short life in obesity. *Nature* **503**, 493–499
16. Wang, L., Gao, P., Zhang, M., Huang, Z., Zhang, D., Deng, Q., Li, Y., Zhao, Z., Qin, X., Jin, D., Zhou, M., Tang, X., Hu, Y., and Wang, L. (2017) Prevalence and ethnic pattern of diabetes and prediabetes in China in 2013. *JAMA* **317**, 2515–2523
17. Badman, M. K., Pissios, P., Kennedy, A. R., Koukos, G., Flier, J. S., and Maratos-Flier, E. (2007) Hepatic fibroblast growth factor 21 is regulated by PPARalpha and is a key mediator of hepatic lipid metabolism in ketotic states. *Cell Metab.* **5**, 426–437
18. Inagaki, T., Dutchak, P., Zhao, G., Ding, X., Gautron, L., Parameswara, V., Li, Y., Goetz, R., Mohammadi, M., Esser, V., Elmquist, J. K., Gerard, R. D., Burgess, S. C., Hammer, R. E., Mangelsdorf, D. J., *et al.* (2007) Endocrine regulation of the fasting response by PPARalpha-mediated induction of fibroblast growth factor 21. *Cell Metab.* **5**, 415–425
19. Lundasen, T., Hunt, M. C., Nilsson, L. M., Sanyal, S., Angelin, B., Alexson, S. E., and Rudling, M. (2007) PPARalpha is a key regulator of hepatic FGF21. *Biochem. Biophys. Res. Commun.* **360**, 437–440
20. Kharitonenkov, A., Shiyanova, T. L., Koester, A., Ford, A. M., Micanovic, R., Galbreath, E. J., Sandusky, G. E., Hammond, L. J., Moyers, J. S., Owens, R. A., Gromada, J., Brozinick, J. T., Hawkins, E. D., Wroblewski, V. J., Li, D. S., *et al.* (2005) FGF-21 as a novel metabolic regulator. *J. Clin. Invest.* **115**, 1627–1635
21. Camporez, J. P., Jornayvaz, F. R., Petersen, M. C., Pesta, D., Guigni, B. A., Serr, J., Zhang, D., Kahn, M., Samuel, V. T., Jurczak, M. J., and Shulman, G. I. (2013) Cellular mechanisms by which FGF21 improves insulin sensitivity in male mice. *Endocrinology* **154**, 3099–3109
22. Perry, R. J., Resch, J. M., Douglass, A. M., Madara, J. C., Rabin-Court, A., Kucukdereli, H., Wu, C., Song, J. D., Lowell, B. B., and Shulman, G. I. (2019) Leptin's hunger-suppressing effects are mediated by the hypothalamic-pituitary-adrenocortical axis in rodents. *Proc. Natl. Acad. Sci. U. S. A.* **116**, 13670–13679
23. Perry, R. J., Wang, Y., Cline, G. W., Rabin-Court, A., Song, J. D., Dufour, S., Zhang, X. M., Petersen, K. F., and Shulman, G. I. (2018) Leptin mediates a glucose-fatty acid cycle to maintain glucose homeostasis in starvation. *Cell* **172**, 234–248.e217
24. Camporez, J. P., Wang, Y., Faarkrog, K., Chukijrungroat, N., Petersen, K. F., and Shulman, G. I. (2017) Mechanism by which arylamine N-acetyltransferase 1 ablation causes insulin resistance in mice. *Proc. Natl. Acad. Sci. U. S. A.* **114**, E11285–E11292
25. Wang, Y., Liu, X., Hou, L., Wu, W., Zhao, S., and Xiong, Y. (2015) Fibroblast growth factor 21 suppresses adipogenesis in pig intramuscular fat cells. *Int. J. Mol. Sci.* **17**, 11
26. Liu, X., Wang, Y., Hou, L., Xiong, Y., and Zhao, S. (2017) Fibroblast growth factor 21 (FGF21) promotes formation of aerobic myofibers via the FGF21-SIRT1-AMPK-PGC1α pathway. *J. Cell Physiol.* **232**, 1893–1906
27. Xiang, Y., Liu, Y., Xiao, F., Sun, X., Wang, X., and Wang, Y. (2020) 2,3,5,6-Tetramethylpyrazine improves diet-induced whole-body insulin resistance via suppressing white adipose tissue lipolysis in mice. *Biochem. Biophys. Res. Commun.* **532**, 605–612